

**EFFECTS OF INDIVIDUAL AND COMBINATION
TREATMENT OF AZITHROMYCIN AND
DOXYCYCLINE ON U87 MALIGNANT GLIOMA
CELL LINE**

SITI NAZIHAHASMA BINTI HASSAN

UNIVERSITI SAINS MALAYSIA

2024

**EFFECTS OF INDIVIDUAL AND COMBINATION
TREATMENT OF AZITHROMYCIN AND
DOXYCYCLINE ON U87 MALIGNANT GLIOMA
CELL LINE**

by

SITI NAZIHAHASMA BINTI HASSAN

**Thesis submitted in fulfilment of the requirements
for the degree of
Doctor of Philosophy**

October 2024

ACKNOWLEDGEMENT

In the name of Allah, the Most Gracious and the Most Merciful, Alhamdulillah. All praise to Allah for guidance and strength to accomplish this endeavour. I am pleased and grateful to Allah for all the blessings bestowed upon me. I navigated through various waves during the process, shaping a better version of myself and a better level of Tawakkul.

I want to thank my main supervisor, Dr. Farizan Ahmad, and my co-supervisors, Assoc. Prof. Abdul Aziz Mohamed Yusoff, Dr. Norhanani Mohd Redzwan, and Prof. Zamzuri Idris, for their steadfast support, keenness, and invaluable knowledge.

I truly thank the staff of Neurosciences, Immunology, Haematology, Pathology, Central Research Laboratory, and Institute of Graduate Studies for their valuable support and facility assistance, as well as Assoc. Prof. Ts. Wan Muhammad Amir W Ahmad, Biostatistician at the Dental School.

I am extremely grateful to my entire family who have always stood by my side, loved, and prayed for me unconditionally. With deep sorrow and the utmost respect, I honour my beloved father, who departed this world on August 4th, 2022, at 4.23 am, after succumbing to a myocardial infarction. I am drowning in a sea of grief, shedding tears for the profound loss that stretches like an endless shadow. His absence, a vacant melody.

Hats off to my superb buddies (especially Izzah Madihah Rosli), the constant companions in the lab, day and night, be it workdays or holidays; you all are the shining stars. Not least of all, special thanks to the Ministry of Higher Education Malaysia through the FRGS (203/PPSP/6171203), USM Fellowship (master's and PhD degrees), and USM Postgraduate Funding Grant (311/PPSP/4404811).

TABLE OF CONTENTS

ACKNOWLEDGEMENT	ii
TABLE OF CONTENTS.....	iii
LIST OF TABLES	ix
LIST OF FIGURES	xi
LIST OF SYMBOLS	xx
LIST OF ABBREVIATIONS	xxii
LIST OF APPENDICES.....	xxx
ABSTRAK.....	xxxi
ABSTRACT	xxxiii
CHAPTER 1 INTRODUCTION.....	1
1.1 Background of the study	1
1.2 Problem statement	3
1.3 Rationale of the study	4
1.4 General objective.....	5
1.4.1 Specific objectives	5
1.5 Research questions	5
1.6 Hypotheses.....	6
CHAPTER 2 LITERATURE REVIEW.....	7
2.1 Brain tumours.....	7
2.2 Glioblastoma	9
2.2.1 Histopathological features.....	10
2.2.2 Molecular biomarkers	12
2.2.3 Treatments and management.....	15
2.3 Therapeutic challenges in glioblastoma.....	17
2.3.1 Cell cycle dysregulation and apoptosis evasion	17

2.3.2	Factors affecting cytotoxic effectiveness	22
2.3.2(a)	Blood-brain barrier.....	22
2.3.2(b)	Tumour heterogeneity	27
2.3.2(c)	Cell plasticity	33
2.3.2(d)	Glioma stem cells.....	35
2.3.2(e)	Tumour microenvironment.....	39
2.3.2(f)	Angiogenesis.....	41
2.4	Drug repurposing approaches for glioblastoma	45
2.4.1	Attributes of antibacterial drugs for anticancer repurposing	45
2.4.1(a)	Azithromycin	46
2.4.1(b)	Doxycycline	51
2.4.2	The underlying rationales of cytotoxic candidates	59
2.4.2(a)	Pharmacological considerations.....	66
2.4.2(b)	Concluding remarks	69
CHAPTER 3	MATERIALS AND METHODS	71
3.1	Study design.....	71
3.2	Chemicals and reagents	73
3.3	Consumables	75
3.4	Apparatus and equipment	76
3.5	Cell culture.....	77
3.5.1	Thawing.....	77
3.5.2	Trypsinisation	78
3.5.3	Counting	78
3.5.4	Cryopreservation.....	79
3.6	Drug dilution	79
3.7	Methods	80
3.7.1	Cell viability assay	81

3.7.1(a) Different drug concentrations	81
3.7.1(b) Different treatment durations.....	81
3.7.1(c) Drug interactions.....	82
3.7.2 Cell survival assay	82
3.7.3 Cell cycle assay.....	83
3.7.3(a) Standard DNA particles.....	84
3.7.3(b) Samples.....	85
3.7.4 Apoptosis assay	86
3.7.4(a) Nuclear staining	86
3.7.4(b) Flow cytometry	87
3.7.4(c) ELISA.....	88
3.7.5 Gene expression assay.....	93
3.7.5(a) RNA extraction	93
3.7.5(b) RNA quantification	94
3.7.5(c) RNA integrity analysis	95
3.7.5(d) cDNA synthesis	95
3.7.5(e) qPCR primers.....	96
3.7.5(f) qPCR components.....	99
3.7.5(g) qPCR conditions	99
3.7.5(h) qPCR efficiency	101
3.7.5(i) qPCR specificity	101
3.7.5(j) Relative quantification	101
3.7.5(k) Ratio calculation	102
3.8 Statistical analyses.....	102
CHAPTER 4 RESULTS.....	104
4.1 Cytotoxicity profiles.....	104
4.1.1 Concentration-response curve	104

4.1.1(a) Temozolomide	104
4.1.1(b) Azithromycin	106
4.1.1(c) Doxycycline	107
4.1.2 Time-response curve	108
4.1.3 Cell morphology and density.....	110
4.1.4 Drug combination interaction.....	115
4.2 Antiproliferation effects.....	118
4.3 Cell cycle division patterns.....	121
4.3.1 Gating strategy.....	121
4.3.2 Flow cytometry analysis.....	123
4.3.3 Inferential analysis.....	125
4.4 Cell death-inducing effects	127
4.4.1 Hoechst labelling	127
4.4.1(a) Morphology analysis	127
4.4.1(b) Frequency analysis	136
4.4.1(c) Inferential analysis	143
4.4.2 Annexin V and PI double labelling.....	145
4.4.2(a) Gating strategy	145
4.4.2(b) Flow cytometry analysis.....	147
4.4.2(c) Inferential analysis	149
4.4.3 Cytochrome C level	151
4.5 Relative mRNA expression.....	152
4.5.1 Transcription factor genes	152
4.5.1(a) TP53	152
4.5.1(b) NF κ B1	154
4.5.2 DNA damage genes	156
4.5.2(a) PRKDC.....	156

4.5.2(b) γ H2AX.....	158
4.5.3 Mitochondrial-mediated fission and fusion genes	160
4.5.3(a) DRP1	160
4.5.3(b) MFN2	162
4.5.4 BCL2 family genes	164
4.5.4(a) BAX	164
4.5.4(b) BAK	166
4.5.4(c) BCL2	168
4.5.4(d) BCLXL.....	170
4.5.5 Ratio analyses	172
4.5.5(a) BAX/BCL2 ratio.....	172
4.5.5(b) BAK/BCL2 ratio.....	173
4.5.5(c) BAX/BCLXL ratio.....	174
4.5.5(d) BAK/BCLXL ratio.....	175
CHAPTER 5 DISCUSSION.....	176
5.1 Cytotoxic effects	176
5.1.1 Concentration-dependent.....	176
5.1.2 Time-dependent	182
5.1.3 Combination interactions	186
5.2 Antiproliferative effects.....	195
5.3 Cytostatic effects	202
5.4 Cell death modes	208
5.5 Molecular analyses	218
5.5.1 Transcription factor genes	219
5.5.2 DNA damage genes	223
5.5.3 Mitochondrial-mediated fission and fusion genes	230
5.5.4 BCL2 family genes	237

**CHAPTER 6 CONCLUSIONS, LIMITATIONS, AND
RECOMMENDATIONS245**

6.1	Conclusions.....	245
6.2	Limitations	247
6.3	Recommendations	247

REFERENCES249

APPENDICES

LIST OF PUBLICATIONS

LIST OF CONFERENCES

LIST OF TABLES

	Page
Table 2.1	Brain tumour prevalence in the Malaysian population 8
Table 2.2	Comparison of brain targeting efficiency of lipid-based nanocarriers 26
Table 2.3	Evidence of tumour cell plasticity shapes phenotypic heterogeneity in GBM 30
Table 2.4	The basic characteristics of GSC subtypes 37
Table 2.5	Preclinical studies of AZI on different cancer cells from 2012 to 2021 48
Table 2.6	AZI-containing regimen in different cancer patient backgrounds 50
Table 2.7	Preclinical studies of DOXY on different cancer cells from 2002 to 2021..... 53
Table 2.8	DOXY-containing regimen in different cancer patient backgrounds..... 57
Table 2.9	Pharmacokinetic parameters of TMZ, AZI, and DOXY 68
Table 3.1	List of chemicals and reagents used in this study..... 73
Table 3.2	List of consumables used in this study 75
Table 3.3	List of apparatus and equipment used in this study 76
Table 3.4	Preparation of the culture medium 77
Table 3.5	Working dilutions of the cytochrome C standard..... 91
Table 3.6	cDNA synthesis components..... 96
Table 3.7	cDNA synthesis steps 96
Table 3.8	Details of the primers used in qPCR..... 97
Table 3.9	qPCR components 99

Table 3.10	qPCR cycling conditions for <i>PRKDC</i> , γ <i>H2AX</i> , <i>DRP1</i> , <i>MFN2</i> , <i>BAX</i> , <i>BAK</i> , and <i>BCLXL</i>	100
Table 3.11	qPCR cycling conditions for <i>TP53</i> , <i>NFκB1</i> , and <i>BCL2</i>	100
Table 4.1	GraphPad Prism-generated best-fit values	105
Table 4.2	GraphPad Prism-generated best-fit values	106
Table 4.3	GraphPad Prism-generated best-fit values	107
Table 4.4	CompuSyn software reports. Summary of the dose-effect curve and Chou-Talalay parameters.....	116
Table 4.5	Relative mRNA expression of <i>TP53</i> and associated values	153
Table 4.6	Relative mRNA expression of <i>NFκB1</i> and associated values	155
Table 4.7	Relative mRNA expression of <i>PRKDC</i> and associated values	157
Table 4.8	Relative mRNA expression of γ <i>H2AX</i> and associated values.....	159
Table 4.9	Relative mRNA expression of <i>DRP1</i> and associated values	161
Table 4.10	Relative mRNA expression of <i>MFN2</i> and associated values.....	163
Table 4.11	Relative mRNA expression of <i>BAX</i> and associated values.....	165
Table 4.12	Relative mRNA expression of <i>BAK</i> and associated values	167
Table 4.13	Relative mRNA expression of <i>BCL2</i> and associated values.....	169
Table 4.14	Relative mRNA expression of <i>BCLXL</i> and associated values	171

LIST OF FIGURES

	Page	
Figure 1.1	Conceptual framework of the study.....	6
Figure 2.1	(a) Haematoxylin and eosin-stained GBM tumour sections reveal a cellular, pleomorphic, glial neoplasm with glomeruloid microvascular proliferation (arrow; 200 \times magnification). (b) Atypical mitotic figures are prominent (arrow; 400 \times magnification). Haematoxylin and eosin-stained sections of another case demonstrate (c) notable nuclear pleomorphism and giant cell features (arrow; 100 \times magnification), along with (d) pseudopalisading necrosis (arrow; 200 \times magnification). Images are from Whitfield and Huse, 2022.	11
Figure 2.2	Overview of selected diffuse gliomas and key diagnostic genes. Adapted from Louis <i>et al.</i> , 2021.....	13
Figure 2.3	Schematic representation of the cell cycle phases along with the respective cyclin-CDK complexes which are necessary for cell cycle progression. G1 (growth phase 1), S (DNA synthesis phase), G2 (growth phase 2), and M, whilst G0 or quiescence (a reversible cycling exit/non-proliferative state). When mitogenic signals trigger proliferation, a complex composed of cyclins and CDKs forms. Abbreviations: PDGF (platelet-derived growth factor); XIAP (x-linked inhibitory apoptosis protein). Adapted from Koliopoulos and Alfieri, 2022; Zhang <i>et al.</i> , 2021.....	21
Figure 2.4	Biological underpinning the emergence of drug resistance. Adapted from Shi <i>et al.</i> , 2023b.	32
Figure 2.5	Phenotypic plasticity via the EMT process is reversible. Adapted from Ramesh <i>et al.</i> , 2020.	34
Figure 2.6	An overview of the hallmark features associated with the therapeutic challenges in GBM.	44

Figure 2.7	Cellular activities affected by mitochondrial dynamics. In general, aberrant mitochondrial dynamics enhance ROS production, and high levels of ROS can modify fusion and fission effectors, forming a feedback loop. Adapted from Ma <i>et al.</i> , 2020.....	60
Figure 2.8	Mitochondrial dynamics in cell cycle (a) and in apoptosis (b), whilst (c) some key proteins and signalling pathways orchestrate mitochondrial fusion and fission. Abbreviations: APAF1 (apoptotic peptidase activating factor 1); AMP-activated protein kinase (AMPK); BAK (BCL2 homologous antagonist killer); CDK1 (cyclin-dependent kinase 1); DRP1 (dynamin-related protein 1); HIF1a (hypoxia-inducible factor 1 subunit alpha); JNK (Jun N-terminal kinase); MFN1/2 (mitofusin 1/2); PKA (protein kinase A). Adapted from Chen <i>et al.</i> , 2023b.....	62
Figure 2.9	Potential therapeutic strategies targeting mitochondria in GBM. Abbreviations: Mdivi-1 (mitochondrial division inhibitor-1); MFF (mitochondrial fission factor); OPA1 (optic atrophy 1); mtDNA (mitochondrial DNA).....	65
Figure 2.10	Factors affecting the therapeutic window of cytotoxic drugs (which may vary to some extent depending on the drug class and distinctive molecular mechanisms of action). Adapted from Rudd, 2023.....	69
Figure 3.1	A summary of research methods.	72
Figure 4.1	The concentration-response curve of TMZ in U87 cells. Cell viability percentages are plotted against treatment concentrations.	105
Figure 4.2	The concentration-response curve of AZI in U87 cells. Cell viability percentages are plotted against treatment concentrations.	106
Figure 4.3	The concentration-response curve of DOXY in U87 cells. Cell viability percentages are plotted against treatment concentrations.	107
Figure 4.4	Effects of TMZ, AZI, DOXY, and AZI+DOXY on U87 cell viability for 24 to 96 h treatment durations. Different from NC (*), DOXY (^), and AZI+DOXY (#): [#] $P < 0.05$ and ^{**/^^} $P < 0.01$	109

Figure 4.5	Morphological alterations and density of U87 cells observed under an inverted light microscope (magnification 10×). (a) Representative after treatment with TMZ, AZI, DOXY, and AZI+DOXY for 24 h compared with the NC group. White dotted circles represent cell shrinkage, rounding, or bubbling. Scale bar 100 μ m.....	111
Figure 4.5	Morphological alterations and density of U87 cells observed under an inverted light microscope (magnification 10×). (b) Representative after treatment with TMZ, AZI, DOXY, and AZI+DOXY for 48 h compared with the NC group. White dotted circles represent cell shrinkage, rounding, or bubbling. Scale bar 100 μ m.....	112
Figure 4.5	Morphological alterations and density of U87 cells observed under an inverted light microscope (magnification 10×). (c) Representative after treatment with TMZ, AZI, DOXY, and AZI+DOXY for 72 h compared with the NC group. White dotted circles represent cell shrinkage, rounding or bubbling, whereas black dotted circles represent flattened cells. Scale bar 100 μ m.....	113
Figure 4.5	Morphological alterations and density of U87 cells observed under an inverted light microscope (magnification 10×). (d) Representative after treatment with TMZ, AZI, DOXY, and AZI+DOXY for 96 h compared with the NC group. White dotted circles represent cell shrinkage and rounding, whereas black dotted circles represent flattened cells. Scale bar 100 μ m.....	114
Figure 4.6	CompuSyn software reports. (a) Dose-effect curve and (b) Corresponding median-effect plot.....	117
Figure 4.7	Effects of TMZ, AZI, DOXY, and AZI+DOXY on U87 cell proliferation. (a) Different from NC (*) and DOXY (^). * $P < 0.05$ and **/^^ $P < 0.01$	119
Figure 4.7	Effects of TMZ, AZI, DOXY, and AZI+DOXY on U87 cell proliferation. Continued (b) Representative of crystal violet-	

stained U87 cell colonies (indicated by white arrows) captured at 5 \times magnification (scale bars = 100 μ m)	120
Figure 4.8 Gating strategy for cell cycle analysis of U87 cells using Cytobank software. (a) Initial cell population selection based on PI vs. SSC-A. (b) Selected total cells from the gated area (a) and (c) Corresponding contour plot. (d) Sub-gating by cell cycle divisions comprises of G0/G1, S, and G2/M phases and (e) Corresponding counts for each cell division.....	122
Figure 4.9 Effects of TMZ, AZI, DOXY, and AZI+DOXY on cellular DNA content and cell cycle division patterns. Representative Cytobank software-generated (a) Contour plots and (b) Corresponding histograms, as estimated by flow cytometry following PI staining. The first and second peaks represent the G0/G1 (blue arrow) and G2/M (grey arrow) phases, respectively; cells in the S phase are located between the two peaks.....	124
Figure 4.10 Effects of TMZ, AZI, DOXY, and AZI+DOXY on U87 cellular DNA content and cell proliferation. Relative percentages of cell populations in the G0/G1, S, and G2/M phases are presented based on the total gated cell numbers. Different from NC (*), AZI (\dagger), DOXY (^), and AZI+DOXY (#): $\dagger P < 0.05$ and $^{**/††/^{^/}#/} P < 0.01$. 126	126
Figure 4.11 Nucleus morphology of U87 cells observed using a confocal microscope (magnification 20 \times). (a) Representative untreated cells. White arrows represent nuclei with vesicular chromatin. Scale bar 100 μ m	128
Figure 4.11 Nucleus morphology of U87 cells observed using a confocal microscope (magnification 20 \times). Continued (b) Representative after treatment with TMZ. White, green, yellow, and red arrows represent nuclei with vesicular chromatin, pyknotic, karyorrhectic, and apoptotic bodies, respectively. Scale bar 100 μ m.....	129
Figure 4.11 Nucleus morphology of U87 cells observed using a confocal microscope (magnification 20 \times). Continued (c) Representative after treatment with AZI. White, green, yellow, and red arrows	

represent nuclei with vesicular chromatin, pyknotic, karyorrhectic, and apoptotic bodies, respectively. Scale bar 100 μm	130
Figure 4.11 Nucleus morphology of U87 cells observed using a confocal microscope (magnification 20 \times). Continued (d) Representative after treatment with DOXY. White, green, yellow, and red arrows represent nuclei with vesicular chromatin, pyknotic, karyorrhectic, and apoptotic bodies, respectively. Scale bar 100 μm	131
Figure 4.11 Nucleus morphology of U87 cells observed using a confocal microscope (magnification 20 \times). Continued (e) Representative after treatment with AZI+DOXY. White, green, yellow, and red arrows represent nuclei with vesicular chromatin, pyknotic, karyorrhectic, and apoptotic bodies, respectively. Scale bar 100 μm	132
Figure 4.12 Nucleus morphology of U87 cells observed using a confocal microscope (magnification 20 \times). (a) Representative after treatment with TMZ, AZI, and DOXY for 24 h compared with the NC group. White, green, yellow, and red arrows represent nuclei with vesicular chromatin, pyknotic, karyorrhectic, and apoptotic bodies, respectively. Scale bar 100 μm	133
Figure 4.12 Nucleus morphology of U87 cells observed using a confocal microscope (magnification 20 \times). Continued (b) Representative after treatment with TMZ, AZI, and DOXY for 72 h compared with the NC group. White, green, yellow, and red arrows represent nuclei with vesicular chromatin, pyknotic, karyorrhectic, and apoptotic bodies, respectively. Scale bar 100 μm	134
Figure 4.13 Analysis of nuclei based on Figure 4.11 (a-e) using ImageJ software. (a) Selected nuclei after auto-binary, watershed, and manual exclusion for the NC group.....	137
Figure 4.13 Analysis of nuclei based on Figure 4.11 (a-e) using ImageJ software. Continued (b) Selected nuclei after auto-binary, watershed, and manual exclusion following treatment with TMZ..	138

Figure 4.13	Analysis of nuclei based on Figure 4.11 (a-e) using ImageJ software. Continued (c) Selected nuclei after auto-binary, watershed, and manual exclusion following treatment with AZI....	139
Figure 4.13	Analysis of nuclei based on Figure 4.11 (a-e) using ImageJ software. Continued (d) Selected nuclei after auto-binary, watershed, and manual exclusion following treatment with DOXY.	140
Figure 4.13	Analysis of nuclei based on Figure 4.11 (a-e) using ImageJ software. Continued (e) Selected nuclei after auto-binary, watershed, and manual exclusion following treatment with AZI+DOXY.....	141
Figure 4.13	Analysis of nuclei based on Figure 4.11 (a-e) using ImageJ software. Continued (f) Nuclei count.	142
Figure 4.14	Analysis of nuclear area based on Figure 4.13 (a-e) using ImageJ software. (a) A rank plot analysis of nuclear area.	144
Figure 4.14	Analysis of nuclear area based on Figure 4.13 (a-e) using ImageJ software. Continued (b) Corresponding pairwise comparisons between groups. Different from NC (*), AZI (†), and DOXY (^): ^ $P < 0.05$ and **/††/^ $P < 0.01$	144
Figure 4.15	Gating strategy for live/dead analysis of U87 cells using FCS 7 Express cytometry software. (a) Initial cell population selection based on FSC-A vs. SSC-A. (b) Selected cells from the gated area (a), and (c) Percentage of viable (Q1), early apoptotic (Q2), late apoptotic (Q3), and necrotic (Q4) U87 cells in the quadrant plot...	146
Figure 4.16	Effects of TMZ, AZI, DOXY and AZI+DOXY on U87 cell death. Representative (a) FSC-A vs. SSC-A flow cytometry analysis of the cell populations. (b) Corresponding Annexin V-FITC vs. PI plots; the lower left quadrant (Q1) indicates the percentage of viable cells, the lower right quadrant (Q2) indicates the percentage of early apoptotic cells, the upper right quadrant (Q3) indicates the percentage of late apoptotic cells, and the upper left quadrant (Q4) indicates the percentage of necrotic cells.....	148

Figure 4.17	Effects of TMZ, AZI, DOXY, and AZI+DOXY on U87 cell death. Relative percentages of viable, apoptotic, and necrotic cell populations are presented based on the total gated cell numbers. Different from NC (*), TMZ (‡), AZI (†), DOXY (^), and AZI+DOXY (#); *†/P < 0.05 and **/††/^\#/## P < 0.01.....	150
Figure 4.18	Effects of TMZ, AZI, DOXY, and AZI+DOXY on cytochrome C levels.....	151
Figure 4.19	Relative mRNA expression of <i>TP53</i> . Gene expression less than and more than 1.0 (---) is downregulated and upregulated, respectively. Different from NC (*), TMZ (‡), AZI (†), and DOXY (^): †/P < 0.05 and **/‡‡ P < 0.01.....	153
Figure 4.20	Relative mRNA expression of <i>NFKB1</i> . Gene expression less than and more than 1.0 (---) is downregulated and upregulated, respectively. Different from NC (*): ** P < 0.01.....	155
Figure 4.21	Relative mRNA expression of <i>PRKDC</i> . Gene expression less than and more than 1.0 (---) is downregulated and upregulated, respectively. Different from NC (*) and AZI (†): † P < 0.05 and **/†† P < 0.01.....	157
Figure 4.22	Relative mRNA expression of <i>γH2AX</i> . Gene expression less than and more than 1.0 (---) is downregulated and upregulated, respectively.....	159
Figure 4.23	Relative mRNA expression of <i>DRP1</i> . Gene expression less than and more than 1.0 (---) is downregulated and upregulated, respectively.....	161
Figure 4.24	Relative mRNA expression of <i>MFN2</i> . Gene expression less than and more than 1.0 (---) is downregulated and upregulated, respectively. Different from NC (*), TMZ (‡), AZI (†), and DOXY (^): ^ P < 0.05 and **/‡‡/†† P < 0.01.....	163
Figure 4.25	Relative mRNA expression of <i>BAX</i> . Gene expression less than and more than 1.0 (---) is downregulated and upregulated, respectively.....	165

Figure 4.26	Relative mRNA expression of <i>BAK</i> . Gene expression less than and more than 1.0 (---) is downregulated and upregulated, respectively.....	167
Figure 4.27	Relative mRNA expression of <i>BCL2</i> . Gene expression less than and more than 1.0 (---) is downregulated and upregulated, respectively. Different from NC (*), TMZ (‡), AZI (†), and DOXY (^\wedge): */‡ $P < 0.05$ and **/‡/†/^\wedge $P < 0.01$	169
Figure 4.28	Relative mRNA expression of <i>BCLXL</i> . Gene expression less than and more than 1.0 (---) is downregulated and upregulated, respectively.....	171
Figure 4.29	Effect of drug treatments on the <i>BAX/BCL2</i> ratio.	172
Figure 4.30	Effect of drug treatments on the <i>BAK/BCL2</i> ratio.	173
Figure 4.31	Effect of drug treatments on the <i>BAX/BCLXL</i> ratio.	174
Figure 4.32	Effect of drug treatments on the <i>BAK/BCLXL</i> ratio.	175
Figure 5.1	A putative schematic diagram on the reduction of cell viability by experimental drugs. Adapted from Ahler <i>et al.</i> , 2013; Luger <i>et al.</i> , 2018; Xiao <i>et al.</i> , 2019; Dijk <i>et al.</i> , 2020.....	181
Figure 5.2	An illustration of possible approaches to targeting GBM cells using AZI and DOXY.	195
Figure 5.3	A putative schematic diagram of the possible events following AZI-, DOXY-, and AZI+DOXY-induced DNA damage. Abbreviation: P (phosphorylation/activation).	207
Figure 5.4	Insights drawn from the present study embrace gaps in knowledge whilst integrating the existing evidence on the probable mode of cell death.	218
Figure 5.5	A putative schematic diagram of the possible interplay of γ <i>H2AX</i> and <i>PRKDC</i> levels under AZI, DOXY, and AZI+DOXY treatments.	229

Figure 5.6	A putative representation of how AZI, DOXY, and AZI+DOXY trigger apoptosis in U87 cells involving mitochondria fission and fusion.....	237
Figure 5.7	A putative representation of mitochondria-mediated apoptosis in U87 cells under AZI, DOXY, and AZI+DOXY treatments.	244
Figure 6.1	Model explaining the putative role of experimental drugs in U87 cells. DNA damage is indicated by increased mRNA levels of <i>TP53</i> , <i>NFKB1</i> , <i>PRKDC</i> , and/or <i>γH2AX</i> ; mitochondrial damage is marked by elevated <i>DRP1</i> and <i>MFN2</i> ; and apoptosis is demonstrated by alterations in the <i>BCL2</i> family, notably an elevated ratio of pro-apoptotic to anti-apoptotic factors.....	246

LIST OF SYMBOLS

α	Significance level
$^{\circ}\text{C}$	Celsius
\pm	Plus-minus
ψ	Pseudoexon
Δ	Absolute precision
\uparrow	Increased levels/induces
\downarrow	Decreased levels/inhibits
\approx	Approximately equal to
∞	Infinity
$\%$	Percentage
cm^2	Square centimetres
Ca^{2+}	Calcium
g	Gram
g/dl	Grams per decilitre
g/mol	Grams per mole
Gy	Gray
h	Hour
H_2O	Water
HCl	Hydrochloride
kg	Kilogram
K^+	Potassium
l	Litre
min	Minutes
ml	Millilitre
mM	Millimolar

mg	Milligram
mmol/l	Millimoles per litre
m	The shape of the dose-effect curve
n	Sample size
NaCl	Sodium chloride
nmol	Nanomoles
nmol/l	Nanomoles per litre
nM	Nanomolar
nt	Nucleotide
ng	Nanogram
NH ₂	Cationic amino
Na ⁺	Sodium
<i>P</i>	Significance value
<i>r</i>	Pearson correlation coefficient
s	Seconds
SiO ₂	Mesoporous silica
T _m	Melting temperature
U	Units of activity
μg	Microgram
μg/ml	Microgram per millilitre
μl	Microlitre
μM	Micromolar
μmol/l	Micromoles per litre
V	Volts
χ ²	Chi-square

LIST OF ABBREVIATIONS

$\Delta\Psi_{\text{mt}}$	Mitochondrial membrane potential
γH2AX	Phosphorylated form of histone H2AX
2D	Two-dimensional
3D	Three-dimensional
AZI	Azithromycin
AUC	Area under curve
ALDH1	Aldehyde dehydrogenase 1
AKT	Protein kinase B
ABC	ATP-binding cassette
AIF	Apoptosis-inducing factor
AP-1	Activator protein 1
ASK	Apoptosis signal-regulated kinase 1
APO 2.7	Apoptosis-related protein 2.7
$A_{260/280}$	Absorbance ratio at 260 and 280 nm
$A_{260/230}$	Absorbance ratio at 260 and 230 nm
ANOVA	Analysis of variance
ATPase	Adenosine triphosphatase
APAF1	Apoptotic peptidase activating factor 1
AMPK	AMP-activated protein kinase
ATM	Ataxia-telangiectasia mutated
BBB	Blood-brain barrier
BAX	BCL2-associated X protein
BAD	BCL2-associated agonist of cell death
BIM	BCL2 interacting mediator of cell death
BCL2	B-cell lymphoma 2

BCLXL	B-cell lymphoma-extra-large
CSCs	Cancer stem cells
Chr	Chromosome
CD44	Cluster of differentiation 44
CI	Combination index
CNS	Central nervous system
c-MYC	Cellular myelocytomatosis
CL	Classical
CDKN2A	Cyclin-dependent kinase inhibitor 2A
ChIP-seq	Chromatin immunoprecipitation sequencing
CRISPR	Clustered regularly interspaced short palindromic repeats
CAFs	Cancer-associated fibroblasts
CHOP	C/EBP homologous protein
CCL2/11	Chemokine (CC motif) ligand 2/11
CXCL1/2/9	Chemokine (CXC motif) ligand 1/2/9
C/EBP β	CCAAT/enhancer binding protein β
CEN	Chicken erythrocyte nuclei
CTN	Calf thymocyte nuclei
cDNA	Complementary DNA
CHEK	Checkpoint kinases
CML	Chronic myeloid leukaemia
CHE	Chelerythrine
DOXY	Doxycycline
DNA	Deoxyribonucleic acid
DDR	DNA damage response
DRI	Dose reduction index
DR 4/5	Death receptor 4/5

DRP1	Dynamin-related protein 1
DSBs	DNA Double-strand breaks
DNA-PKcs	DNA-dependent protein kinase catalytic subunit
DLBCL	Diffuse large B-cell lymphoma
DMSO	Dimethyl sulfoxide
DMEM	Dulbecco's modified Eagle's medium
DPBS	Dulbecco's phosphate-buffered saline
DF	Dilution factor
DFNA5	Deafness, autosomal dominant 5
EGFR	Epidermal growth factor receptor
ECM	Extracellular matrix
EMT	Epithelial-mesenchymal transition
ERK	Extracellular signal-regulated kinase
ETC	Electron transport chain
e.g.,	<i>Exempli gratia</i> or for example
ECs	Endothelial cells
FDA	Food and Drug Administration
FACS	Fluorescence-activated cell sorting
Fas	TNF receptor superfamily member 6
FasL	Fas ligand
FADD	FAS-associated death domain protein
Fu	Fraction of unaffected cells
Fa	Fraction of affected cells
FL	Fluorescence
FITC	Fluorescein isothiocyanate
GBM	Glioblastoma
GSCs	Glioma stem cells

GSH	Glutathione
GOI	Gene of interest
gDNA	Genomic DNA
HGG	High-grade glioma
HPLC	High-performance liquid chromatography
HIF1a	Hypoxia-inducible factor 1 subunit alpha
i.e.,	<i>Id est</i> or that is
IDH	Isocitrate dehydrogenase
IPS	Institut Pengajian Siswazah
IC ₅₀	Half-maximal inhibitory concentration
IR	Ionising radiation
JNK	c-Jun N-terminal kinase
KD	Knockdown
KO	Knockout
LGG	Low-grade glioma
LC3B	Microtubule-associated protein 1 light chain 3 beta
LPA	Lysophosphatidate
LMP	Lysosomal membrane permeabilisation
MG	Malignant glioma
mut	Mutant
MGMT	O6-methylguanine-DNA methyltransferase
MYC	Myelocytomatosis
MES	Mesenchymal
mRNA	Messenger RNA
mtDNA	Mitochondrial DNA
MIC	Minimum inhibitory concentration
MTT	3-(4, 5-dimethylthiazol-2-yl)-2, 5-diphenyltetrazolium bromide

MERFISH	Multiplexed error-robust fluorescence in situ hybridisation
MFN1/2	Mitofusin 1/2
Med	Medium
MAPK3	Mitogen-activated protein kinase 3
MCL1	Myeloid cell leukaemia 1
MMPs	Matrix metalloproteinases
MMP9	Matrix metalloproteinase 9
Mdivi-1	Mitochondrial division inhibitor 1
MFF	Mitochondrial fission factor
MTCO1/2	Mitochondrial-encoded cytochrome c oxidase subunit 1/2
MTATP6/8	Mitochondrial-encoded ATP synthase membrane subunit 6/8
NR	Not reported
NLRP3	NLR family pyrin domain containing 3
NRF1/2	Nuclear respiratory factor 1/2
NFκβ	Nuclear factor-kappa β
NF1	Neurofibromatosis 1
NC	Negative control
NBF	Neutral buffered formalin
NTC	Non-template control
NEAA	Non-Essential Amino Acids
NAC	N-acetyl-L-cysteine
OS	Overall survival
OPA1	Optic atrophy 1
PN	Proneural
PEG	Polyethylene glycol
PKA	Protein kinase A
PFS	Progression-free survival

PLGA	Poly (lactic-co-glycolic acid)
p53	Tumour protein p53
P-gp	P-glycoprotein
PDGF	Platelet-derived growth factor
PDOX	Patient-derived orthotopic xenograft
p-STAT3	Phosphorylated signal transducer and activator of transcription 3
p62	Sequestosome 1
PCL	Polycaprolactone
PARP	Poly-ADP-ribose polymerase
p-VEGFR2	Phosphorylated vascular endothelial growth factor receptor 2
p-FAK	Phosphorylated focal adhesion kinase
p-PI3K	Phosphorylated phosphatidylinositol 3 kinase
p-AKT	Phosphorylated protein kinase B
p-eIF2 α	Phosphorylated eukaryotic initiation factor 2 α
p-FAK	Phosphorylated focal adhesion kinase
p38MAPK	p38 mitogen-activated protein kinase
PUMA	p53 upregulated modulator of apoptosis
p21	Cyclin-dependent kinase inhibitor
PI	Propidium iodide
P	Phosphorylation
PIKK	Phosphatidylinositol 3-kinase-related kinase
PDT	Potentiating photodynamic therapy
QC	Quality control
qPCR	Quantitative real-time PCR
ROS	Reactive oxygen species
RNA	Ribonucleic acid
RTK	Receptor tyrosine kinase

RAF1	Raf-1 proto-oncogene, serine/threonine kinase
RT	Room temperature
rpm	Revolutions per minute
RT	Reverse transcription
scRNA-seq	Single-cell RNA sequencing
snRNA-seq	Single nuclei RNA sequencing
scATAC-seq	Single-cell assay for transposase-accessible chromatin with high-throughput sequencing
SOD2	Mitochondrial superoxide dismutase 2
Smac	Second mitochondria-derived activator of caspases
SHH	Sonic Hedgehog
SNAI1/2	Snail family transcriptional repressor 1/2
SPSS	Statistical package for social sciences
TMZ	Temozolomide
TERT	Telomerase reverse transcriptase
TME	Tumour microenvironment
TAMs	Tumour-associated microglia/macrophages
TNF α	Tumour necrosis factor α
TGF β 1	Transforming growth factor beta 1
TI	Therapeutic index
THG	Thermogel
TIMP2	Tissue inhibitor of metalloproteinase 2
TFAM	Mitochondrial transcription factor A
TRAIL	TNF-related apoptosis-inducing ligand
TWIST1/2	Twist family BHLH transcription factor 1/2
TP53	Tumour protein p53 gene
TTCC	T-type calcium channel
TUNEL	Terminal deoxynucleotidyl transferase dUTP nick end labelling

USM	Universiti Sains Malaysia
USLP	Ultra-small, large pore silica
VEGF	Vascular endothelial growth factor
vs.	versus
WHO	World Health Organization
wt	Wild-type
WNT	Wingless-related integration site

LIST OF APPENDICES

APPENDIX A	AUTOMATED CELL COUNTING
APPENDIX B	PREPARATION OF WORKING MTT SOLUTION
APPENDIX C	PREPARATION OF WORKING CRYSTAL VIOLET DYE SOLUTION AND U87 COLONIES ON DAY 25
APPENDIX D	CELL CYCLE KIT DETAILS, STANDARD DNA ANALYSIS, AND CV BAR CHART
APPENDIX E	PREPARATION OF WORKING HOECHST 33342 DYE SOLUTION
APPENDIX F	APOPTOSIS ASSAY KIT DETAILS AND REAGENT PREPARATION
APPENDIX G	HUMAN CYTOCHROME C SIMPLE STEP ELISA KIT DETAILS, DF DETERMINATION OF PROTEIN SAMPLES, AND REPRESENTATIVE STANDARD PLUS SAMPLES
APPENDIX H	DNA EXTRACTION KIT DETAILS AND REAGENT PREPARATION
APPENDIX I	SPECTROPHOTOMETRIC QUANTIFICATION OF RNA SAMPLES
APPENDIX J	ELECTROPHORETIC ANALYSIS OF RNA SAMPLES
APPENDIX K	PREPARATION OF AGAROSE GEL, BUFFERS, DNA DYE, DNA LADDER, AND DNASE I TREATMENT SOLUTION
APPENDIX L	CHEMICAL PROPERTIES AND PREPARATION OF PRIMERS
APPENDIX M	ANALYSIS OF qPCR EFFICIENCY
APPENDIX N	ANALYSIS OF REFERENCE GENE (GAPDH) STABILITY
APPENDIX O	REPRESENTATIVE OF AMPLIFICATION PLOT
APPENDIX P	REPRESENTATIVE OF MELTING CURVE ANALYSIS
APPENDIX Q	ELECTROPHORETIC ANALYSIS OF qPCR PRODUCTS

**KESAN RAWATAN AZITHROMYCIN DAN DOXYCYCLINE
SECARA INDIVIDU DAN KOMBINASI PADA TITISAN SEL MALIGNAN
GLIOMA U87**

ABSTRAK

Glioblastoma (GBM) adalah tumor otak malignan primer yang paling prevalen dikalangan orang dewasa. Rawatan konvensional, termasuk kombinasi kemoterapi temozolomide (TMZ) dan radioterapi, hanya memberikan kelangsungan hidup yang minimum. Rintangan terhadap terapi-terapi ini bukan sahaja kerap berlaku, malah dijangka. Berdasarkan bukti yang kukuh bahawa azithromycin (AZI) dan doxycycline (DOXY) menyebabkan sitotoksiti yang berkaitan dengan apoptosis dalam pelbagai model kanser *in vitro* dan *in vivo*, ubat-ubatan ini telah dipilih untuk kajian ini. Potensi antikanser mereka, sama ada secara individu dan kombinasi, dinilai menggunakan titisan sel malignan glioma U87, khususnya GBM. Kajian *in vitro* ini mengukur daya hidup sel, bilangan koloni, interaksi sitotoksik, taburan kitaran sel, morfologi nukleus, pecahan kematian sel, aras sitokrom C, dan ekspresi gen yang berhubung dengan sitotoksiti dan apoptosis. Ujian *3-(4,5-dimethylthiazol-2-yl)-2,5-diphenyltetrazolium bromide* menunjukkan bahawa keberkesanan AZI (IC_{50} : 92.0 $\mu\text{g/ml}$) lebih tinggi berbanding TMZ (IC_{50} : 151.0 $\mu\text{g/ml}$) dan DOXY (IC_{50} : 147.0 $\mu\text{g/ml}$) dalam sel U87. Berbanding dengan rawatan tunggal, AZI+DOXY (92.0+147.0 $\mu\text{g/ml}$) tidak menunjukkan peningkatan sitotoksiti pada pelbagai kepekatan dan tempoh masa, dan bukti menunjukkan interaksi antagonistik. Berdasarkan ujian kelangsungan hidup sel, AZI menunjukkan kesan antiproliferatif yang signifikan secara statistik berbanding dengan kawalan negatif (NC) dan DOXY, tetapi hanya dengan NC di bawah TMZ. Analisis sitometri aliran menggunakan pelabelan propidium iodida (PI) menunjukkan

bahawa AZI tidak mengubah kitaran sel, manakala TMZ dan DOXY atau AZI+DOXY masing-masing menghentikan sel dalam fasa S/G2/M dan G0/G1. Pewarnaan Hoechst 33342 menunjukkan ciri-ciri apoptosis dalam nukleus sel di semua kumpulan rawatan, namun luas nuklear yang lebih besar diperhatikan berbanding dengan NC. Selanjutnya, analisis sitometri aliran menggunakan pelabelan Annexin V/PI menunjukkan bahawa apoptosis merupakan bentuk utama kematian sel yang diinduksi oleh TMZ dan AZI. Sebaliknya, DOXY dan AZI+DOXY merangsang kedua-dua apoptosis dan nekrosis. Analisis spektrofotometrik aras protein sitokrom C menunjukkan peningkatan dalam semua kumpulan rawatan. Pada tahap transkripsi, semua rawatan meningkatkan aras ekspresi mRNA *TP53* dan *NFKB1*, dengan AZI+DOXY secara signifikan merangsang kedua-dua gen. Aras *PRKDC* meningkat dengan ketara dengan TMZ, DOXY, dan AZI+DOXY. Sebaliknya, aras *γH2AX* adalah lebih tinggi dalam kumpulan AZI berbanding dengan semua rawatan yang lain. Aras ekspresi mRNA *DRP1* dan *MFN2* meningkat dalam semua kumpulan rawatan, dengan AZI+DOXY yang secara ketara menginduksi *MFN2*. Selain itu, hanya AZI yang meningkatkan kedua-dua aras *BAX* dan *BAK*, manakala *BCL2* meningkat secara signifikan dalam kumpulan AZI dan AZI+DOXY, dan AZI+DOXY menunjukkan aras *BCLXL* terendah di antara kumpulan rawatan. Tambahan lagi, AZI meningkatkan nisbah *BAX/BCL2*, *BAK/BCL2*, dan *BAX/BCLXL*, manakala AZI+DOXY menunjukkan nisbah tertinggi bagi *BAK/BCLXL*. Kesimpulannya, AZI menunjukkan aktiviti antikanser dengan menghalang proliferasi sel, sebahagiannya melalui induksi apoptosis. Sebaliknya, DOXY dan AZI+DOXY menginduksi pemberhentian kitaran sel dan kedua-dua apoptosis dan nekrosis sebagai sebahagian daripada mekanisma antikanser mereka. Namun, rawatan dengan ubat-ubatan eksperimen secara individu memberikan kesan antikanser yang optimum berbanding kombinasi.

**EFFECTS OF INDIVIDUAL AND COMBINATION TREATMENT OF
AZITHROMYCIN AND DOXYCYCLINE ON U87 MALIGNANT GLIOMA
CELL LINE**

ABSTRACT

Glioblastoma (GBM) is the most prevalent malignant primary brain tumour in adults. Conventional treatment, which includes concurrent temozolomide (TMZ) chemotherapy and radiotherapy, provides only marginal survival benefits. Resistance to these therapies is both common and anticipated. Given the compelling evidence that azithromycin (AZI) and doxycycline (DOXY) induce apoptosis-related cytotoxicity in various cancer models *in vitro* and *in vivo*, these drugs were chosen for the present study. Their anticancer potential, both alone and in combination, was evaluated using the U87 malignant glioma cell line, specifically GBM. This *in vitro* study assessed cell viability, colony numbers, cytotoxic interactions, cell cycle distributions, nuclear morphology, cell death fractions, cytochrome C levels, and gene expression related to cytotoxicity and apoptosis. The *3-(4,5-dimethylthiazol-2-yl)-2,5-diphenyltetrazolium bromide* assay showed that AZI (IC_{50} : 92.0 μ g/ml) exhibited greater potency compared to TMZ (IC_{50} : 151.0 μ g/ml) and DOXY (IC_{50} : 147.0 μ g/ml) in U87 cells. Compared to single-drug treatments, AZI+DOXY (92.0+147.0 μ g/ml) did not show increased cytotoxicity across various concentrations and time points, and evidence indicated an antagonistic interaction. Based on the cell survival assay, AZI exhibited a statistically significant antiproliferative effect compared to the negative control (NC) and DOXY, but only to NC under TMZ. Flow cytometric analysis using propidium iodide (PI) labelling revealed that AZI did not interfere with the cell cycle, whereas TMZ and DOXY or AZI+DOXY arrested cells in the S/G2/M and G0/G1 phases, respectively.

Hoechst 33342 staining revealed apoptotic features in cell nuclei across all treatment groups; however, a larger nuclear area was observed than that of NC. Furthermore, flow cytometric analysis using Annexin V/PI labelling indicated that apoptosis was the predominant form of cell death induced by TMZ and AZI. In contrast, DOXY and AZI+DOXY induced both apoptosis and necrosis. Spectrophotometric analysis of cytochrome C protein levels exhibited an increase across all treatment groups. At the transcriptional level, all treatments enhanced *TP53* and *NFKB1* mRNA expression levels, with AZI+DOXY significantly inducing both genes. *PRKDC* levels markedly increased with TMZ, DOXY, and AZI+DOXY. In contrast, *γH2AX* levels were higher in the AZI group than in any of the other treatments. *DRP1* and *MFN2* mRNA expression levels were elevated across all treatment groups, with AZI+DOXY substantially induced *MFN2*. Moreover, only AZI enhanced both *BAX* and *BAK* levels, whilst *BCL2* significantly increased in the AZI and AZI+DOXY groups, and AZI+DOXY showed the lowest *BCLXL* levels among the treatment groups. Additionally, AZI increased the ratios of *BAX/BCL2*, *BAK/BCL2*, and *BAX/BCLXL*, whereas AZI+DOXY exhibited the highest ratio of *BAK/BCLXL*. In short, AZI shows anticancer activity by inhibiting cell proliferation, in part through the induction of apoptosis. On the other hand, DOXY and AZI+DOXY induce cell cycle arrest and both apoptosis and necrosis as part of their anticancer mechanisms. However, the experimental drugs appear to yield optimal anticancer effects when given alone rather than concurrently.

CHAPTER 1

INTRODUCTION

1.1 Background of the study

Cancer is a malignant tumour defined by the unchecked and rapid proliferation of aberrant cells that have evaded apoptosis (programmed cell death), invaded nearby tissues, and metastasised to different parts of the body. It can arise in almost any organ and tissue and, is a growing cause of mortality (occurring between ages 30–70 years) worldwide (Bray *et al.*, 2021). According to GLOBOCAN estimates, cancer deaths climbed to 9.9 million in 2020, up from 9.5 in 2018, and there were 19.3 million new cancer cases in 2020, with a projected 28.4 million in 2040 (Ferlay *et al.*, 2019; Ferlay *et al.*, 2021; Sung *et al.*, 2021).

Among the 36 human cancers worldwide in 2020, brain and central nervous system (CNS) cancers accounted for approximately 308,102 (1.6% of all sites) new cases and 251,329 (2.5% of all sites) new deaths (Sung *et al.*, 2021). In the Malaysian population from 2012 to 2016, it was recorded as one of the ten most common cancers among Malays but not Chinese or Indians. The number of cases was 642 (2.9%) in males and 557 (1.9%) in females (Azizah *et al.*, 2019). The global incidence rate is 3.9 per 100,000 males and 3.0 per 100,000 females, whereas in Malaysia, it is 1.8 per 100,000 males and 1.6 per 100,000 females (Azizah *et al.*, 2019; Sung *et al.*, 2021).

Globally, glioblastoma (GBM) is the most common primary brain tumour in adults. This type of high-grade glioma (HGG), often referred to as the most malignant glioma, is extremely lethal, exhibiting a high degree of plasticity, heterogeneity, and infiltrativeness (Neftel *et al.*, 2019; Yabo *et al.*, 2022). Despite countless clinical trials and research advancements, it remains refractory to improvements in treatment. Even

with the most promising agents, high failure rates in clinical trials are observed, and resistance to targeted therapies is mainly attributed to intricate interferences between signalling pathways and biological processes (Gatto *et al.*, 2023).

Historically, patient survival rates have been poor, with temozolomide (TMZ)-containing regimens showing the best clinical performance (Guo *et al.*, 2023a). TMZ was first authorised by the Food and Drug Administration (FDA) in 1999 as a second-line therapy for GBM. Following favourable results from a phase III clinical trial commenced by the European Organisation for Research and Treatment of Cancer and the National Cancer Institute of Canada in 2005, the FDA and European Medicines Agency approved TMZ as a first-line treatment for newly diagnosed GBM (Stupp *et al.*, 2009; Stupp *et al.*, 2005). Other FDA-approved options, including nitrosoureas (such as lomustine and carmustine wafer implants), bevacizumab, and tumour-treating fields, may offer survival benefits when used in a combinatorial approach (Narsinh *et al.*, 2024; Obrador *et al.*, 2024).

Given the suboptimal clinical outcomes, numerous pursuits are underway to discover and develop drugs with better efficacy and potency as potential alternatives and adjuvants to current therapies. This includes drug repositioning (also called drug repurposing), which involves the investigation of existing drugs for new therapeutic purposes (O'Rawe *et al.*, 2022). Another ongoing effort involves exploring drug combinations to capitalise on synergistic interactions—increasing therapeutic efficacy at lower doses and thereby reducing systemic toxicity (Hassan *et al.*, 2022; Yang *et al.*, 2023b). Notwithstanding, not all patients favourably respond to the same effective drugs, and even if they do, resistance and relapse remain possible.

Among the attractive candidates under investigation for potential in cancer therapy are azithromycin (AZI) and doxycycline (DOXY). Both antibacterial drugs

have been therapeutically utilised for over four decades (Bright and Hauske, 1984; Cunha *et al.*, 1982). On the other hand, compelling evidence underscores the ability of AZI and DOXY to effectively interfere with tumour growth and progression (Ghasemi and Ghasemi, 2022; Hassan *et al.*, 2023b). Their cytotoxic, antiproliferative, and/or pro-apoptotic effects have been demonstrated in various cancer models, including breast (Akhunzianov *et al.*, 2023), colon (Alshaman *et al.*, 2022; Qiao *et al.*, 2018), gastric (Pandian *et al.*, 2020; Zhou *et al.*, 2012), and lung (Alsaadi *et al.*, 2021; Toriyama *et al.*, 2024). Notably, both AZI and DOXY can eradicate cancer stem cells (CSCs) and preferentially inhibit cancer cells (Lamb *et al.*, 2015b; Peiris-Pagès *et al.*, 2019).

Armed with the existing knowledge, this study aimed to assess the anticancer potential of AZI and DOXY, both individually and in combination, using the human U87 malignant glioma cell line. This cell line is among the most widely used *in vitro* models of GBM in drug screening and mechanistic studies (Mousavi *et al.*, 2023; Wang *et al.*, 2022b; Zhang *et al.*, 2024). U87 cells proliferate rapidly and tend to form neurosphere-like clusters or colonies, reflecting their highly tumourigenic nature (Diao *et al.*, 2019). Furthermore, U87 cells are sensitive to TMZ and well-characterised, with key features of human GBM, including wild-type (wt)-isocitrate dehydrogenase (*IDH*) and wt-tumour protein 53 (*TP53*) (Wang *et al.*, 2017a; Zhang *et al.*, 2024). Overall, the cell line provides consistent and reproducible results across different laboratories, crucial for comparative studies and validating the effects of experimental drugs.

1.2 Problem statement

Current FDA-approved therapies for GBM, which primarily involve surgery followed in sequence by RT with concomitant and adjuvant TMZ, yield only marginal

improvements in survival. Infiltrative growth, tumour heterogeneity, overexpressed efflux pumps, brain anatomical characteristics, and drug resistance critically limit the effectiveness of GBM interventions. Ironically, all GBM cells, not exclusively glioma stem cells (GSCs), exhibit plasticity—undergoing molecular and phenotypic changes that allow them to resist cytotoxicity and evade apoptotic programmes. Moreover, enhanced glycolysis, often misconstrued to support cancer cell proliferation, is indeed insufficient without concurrent mitochondrial metabolism. GSCs display a greater reliance on oxidative phosphorylation (OXPHOS). Collectively, single-agent therapy is highly susceptible to resistance, a challenge further compounded by compensatory mechanisms and stromal components that serve as building blocks for tumour growth, survival, and progression.

1.3 Rationale of the study

Mitochondrial-targeting drugs represent a promising approach to addressing the unmet clinical needs of GBM. This is particularly crucial as virtually all patients eventually relapse and develop resistance to TMZ, resulting in a worsened prognosis and limited treatment options. AZI and DOXY may effectively inhibit GBM growth and progression through various action points, including antiproliferative and pro-apoptotic effects. Notably, both drugs induce cytotoxicity in differentiated tumour cells and suppress CSC proliferation by triggering mitochondrial damage-mediated apoptosis and reducing OXPHOS (Lamb *et al.*, 2015b; Xiao *et al.*, 2019). However, their potential against GBM, whether used alone or in combination, remains largely unexplored. In consensus, it appears that combinatorial approaches are emerging as the winning strategies for tackling the intricate interplay of tumour elements. Unlike single-drug therapies, combination treatments have the potential to enhance potency

and efficacy through synergistic interactions. This modality may also help reduce systemic toxicity and delay the development of resistance. Given their availability, affordability, and extensive clinical safety record, making them therapeutic options would be feasible globally if proven beneficial.

1.4 General objective

To study the anticancer effects of AZI and DOXY alone and in combination on an *in vitro* model of human U87 GBM cells.

1.4.1 Specific objectives

- i. To determine the cytotoxic and proliferation effects in U87 cells following AZI, DOXY, and AZI+DOXY treatments.
- ii. To evaluate the cell cycle effects in U87 cells following AZI, DOXY, and AZI+DOXY treatments.
- iii. To determine the apoptosis effects in U87 cells following AZI, DOXY, and AZI+DOXY treatments.
- iv. To assess the cytotoxic- and apoptosis-associated gene expression effects in U87 cells following AZI, DOXY, and AZI+DOXY treatments.

1.5 Research questions

- i. What are the cytotoxic and proliferation effects of AZI, DOXY, and AZI+DOXY treatments on U87 glioblastoma cells?
- ii. How do AZI, DOXY, and AZI+DOXY treatments affect the cell cycle phases in U87 glioblastoma cells?

- iii. What are the apoptosis-inducing effects of AZI, DOXY, and AZI+DOXY treatments on U87 glioblastoma cells?
- iv. How do AZI, DOXY, and AZI+DOXY treatments alter the expression of cytotoxicity- and apoptosis-associated genes in U87 glioblastoma cells?

1.6 Hypotheses

The hypothesis in this study proposes that AZI, DOXY, and their combined treatment exhibit antiproliferative effects by inducing cell cycle arrest and apoptosis in GBM cells. Moreover, it suggests that the synergistic impact of combined AZI+DOXY treatments is more effective in inhibiting GBM cell growth. Figure 1.1 shows the conceptual framework of the study.

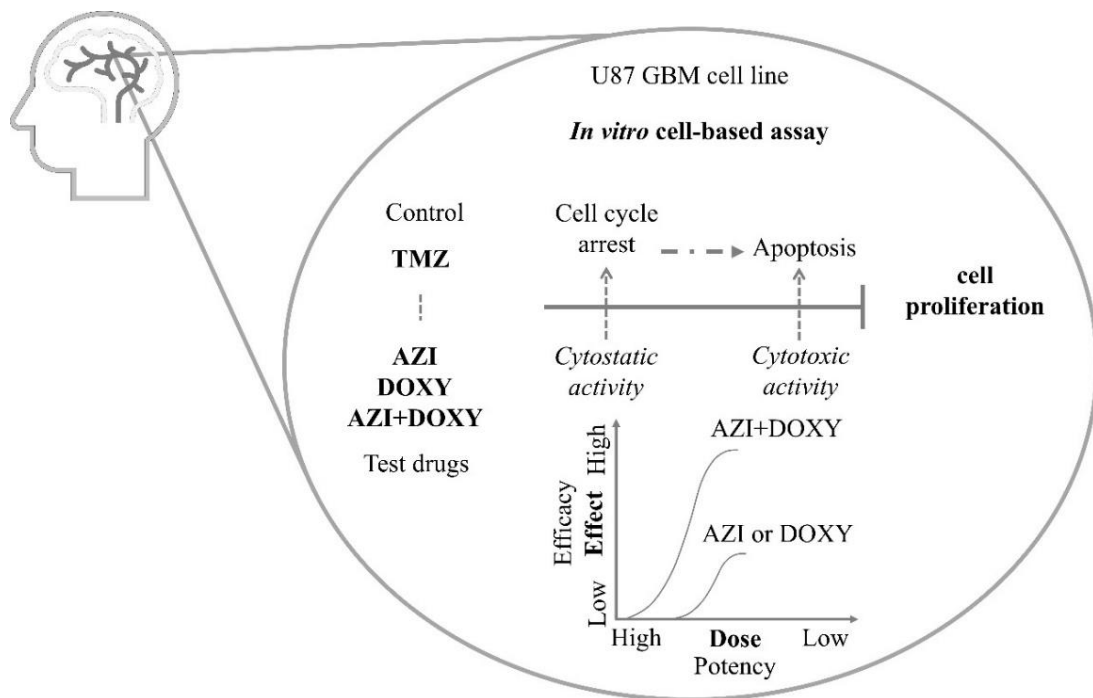


Figure 1.1 Conceptual framework of the study.

CHAPTER 2

LITERATURE REVIEW

2.1 Brain tumours

Brain tumour is a general term for benign or malignant tumours arising from brain tissues—collectively referring to primary CNS tumours. In Southeast Asia, the incidence rates of benign and malignant brain tumours were 6.97 and 3.29 per 100,000 person-years, respectively (Bell *et al.*, 2019). Globally, gliomas and meningiomas are among the most prevalent types of brain tumours (Salari *et al.*, 2023). In the United States, for instance, gliomas rank as the most common primary brain tumours in both children and adults, with GBM accounting for 50.1% of all malignant tumours. GBM is relatively more common in older adults and less so in children (Ostrom *et al.*, 2022a; Ostrom *et al.*, 2022b). Gliomas (61.8%) predominantly occur in the supra-tentorium (frontal, temporal, parietal, and occipital lobes combined), with only a minor fraction identified in CNS regions other than the brain (Ostrom *et al.*, 2022a). Notably, 52.5% of GBM had invaded more than one lobe, with the frontal and temporal lobes being the most frequently affected regions (Guo *et al.*, 2023b).

In Malaysia, a single-centre cross-sectional study showed that the number of brain tumour cases was lower among children (0 to 10 years old), with only 4.4% ($n=17$) from 2013 to 2018 (Othman *et al.*, 2020), whilst 3.5% ($n=8$) from 2018 to 2021 (Heng *et al.*, 2023). From 2009 to 2019, a total of five brain tumour cases were detected in the age range of 0 to 14 years, accounting for 8.2% of all incidents (Azman *et al.*, 2022). In addition, there were 31 cases (14.4%) of brain tumours under the age of 15 from 2011 to 2014 (Dzali *et al.*, 2017). Despite this, the incidence of brain tumours

rises with age, with glioma being the second most common (Heng *et al.*, 2023). Table 2.1 summarises cross-sectional studies on brain tumours in Malaysians.

Table 2.1 Brain tumour prevalence in the Malaysian population

Enrolment time	Commonness			Reference
	Type, % (n)	Age (years), % (n)	Gender, % (n)	
2018–2021	Meningioma, 38.7 (89)	51–60, 34.8 (80)	Female, (132)	57.4 (Heng <i>et al.</i> , 2023)
2009–2019	GBM, 29.5 (18)	40–70, 55.7 (34)	Male, 59.0 (36)	(Azman <i>et al.</i> , 2022)
2013–2018	Meningioma, 27.2 (105)	51–60, 26.2 (101)	Female, (214)	55.5 (Othman <i>et al.</i> , 2020)
2011–2014	Meningioma, 32.7 (71)	>45, 49.8 (107)	Female, (117)	53.9 (Dzali <i>et al.</i> , 2017)

It is important to note that gliomas in children differ substantially from those in adults in terms of prognosis (clinically) and pathobiology (molecularly). The most recent revision, the 5th edition of the WHO classification of the CNS (WHO CNS5), divides them into four different families: (1) Adult-type diffuse gliomas (the majority of primary brain tumours in adults is wt-*IDH* GBM); (2) Paediatric-type diffuse low-grade gliomas (LGG) (expected to have good prognoses); (3) Paediatric-type diffuse HGG (expected to behave aggressively); and (4) Circumscribed astrocytic gliomas (“circumscribed” referring to their more solid growth pattern, as opposed to the inherently “diffuse” tumours in groups 1, 2, and 3) (Louis *et al.*, 2021). For astrocytic tumours, LGG are classified as grades 1 and 2, whilst HGG correspond to grades 3 and 4.

Of particular concern, the burden is increasing worldwide, with gliomas and GBM being the most financially draining (Khanmohammadi *et al.*, 2023). Globally, from 1990 to 2019, the incidence, deaths, and disability-adjusted life years associated

with brain and CNS cancers climbed noticeably (Fan *et al.*, 2022). Notably, in 2016, Indonesia, Thailand, and the Philippines recorded the highest incidence and death rates from primary brain tumours, with Malaysia ranking sixth in both measures. Moreover, scientific output on brain tumours does not reflect the current reality in Southeast Asia. Singapore contributes the majority of articles (44.8%), followed by Thailand (28.0%) and Malaysia (20.6%) (Mondia *et al.*, 2020).

2.2 Glioblastoma

GBM is a rapidly growing cancer that relentlessly diffuses throughout the brain parenchyma and external blood vessel walls, without radiologic or histologic evidence of a less malignant precursor lesion (Ohgaki and Kleihues, 2013). In times before the era of integrated histopathology-molecular analysis, a tumour specimen that did not exhibit the classic histological features of GBM would have been assigned a lower WHO grade (Wen *et al.*, 2020). At present, tumour entities are designated as “not otherwise specified” when molecular data are unavailable (Osborn *et al.*, 2022). Note that the term “glioblastoma multiforme” has been dropped from the WHO CNS5, and “GBM” is no longer used in the context of paediatric-type neoplasms (Louis *et al.*, 2021). However, “glioblastoma multiforme” is still commonly used to refer to wt-*IDH* GBM. The term “multiforme” was originally coined to describe the heterogeneous cellular organisation and histological appearance of the tumour. In this study, “GBM” refers to wt-*IDH* GBM, unless otherwise specified.

2.2.1 Histopathological features

GBM is classified as a CNS WHO grade 4 tumour. Since CNS tumour grading differs from other tumour grading systems, WHO CNS5 endorses the use of the term “CNS WHO grade” for assigning grades and is no longer restricted to histological grades alone. Furthermore, WHO CNS5 has amended two specific aspects of CNS tumour grading. It now uses Arabic numerals (instead of Roman numerals), and neoplasms are graded within types (rather than across different tumour types) (Louis *et al.*, 2021; Louis *et al.*, 2020).

Histopathologically, GBM exhibits diffusely infiltrative growth, an astroglial appearance with angulated nuclei and irregular chromatin, and poor differentiation with brisk mitotic activity. Florid microvascular proliferation and/or necrosis, with or without pseudopalisading, are frequently observed (see Figure 2.1) (Wen *et al.*, 2020; Whitfield and Huse, 2022). Notably, microvascular proliferation and/or necrosis are both sufficient criteria to establish the diagnosis of GBM in adult wt-*IDH* diffuse and astrocytic gliomas (Louis *et al.*, 2021; Whitfield and Huse, 2022).

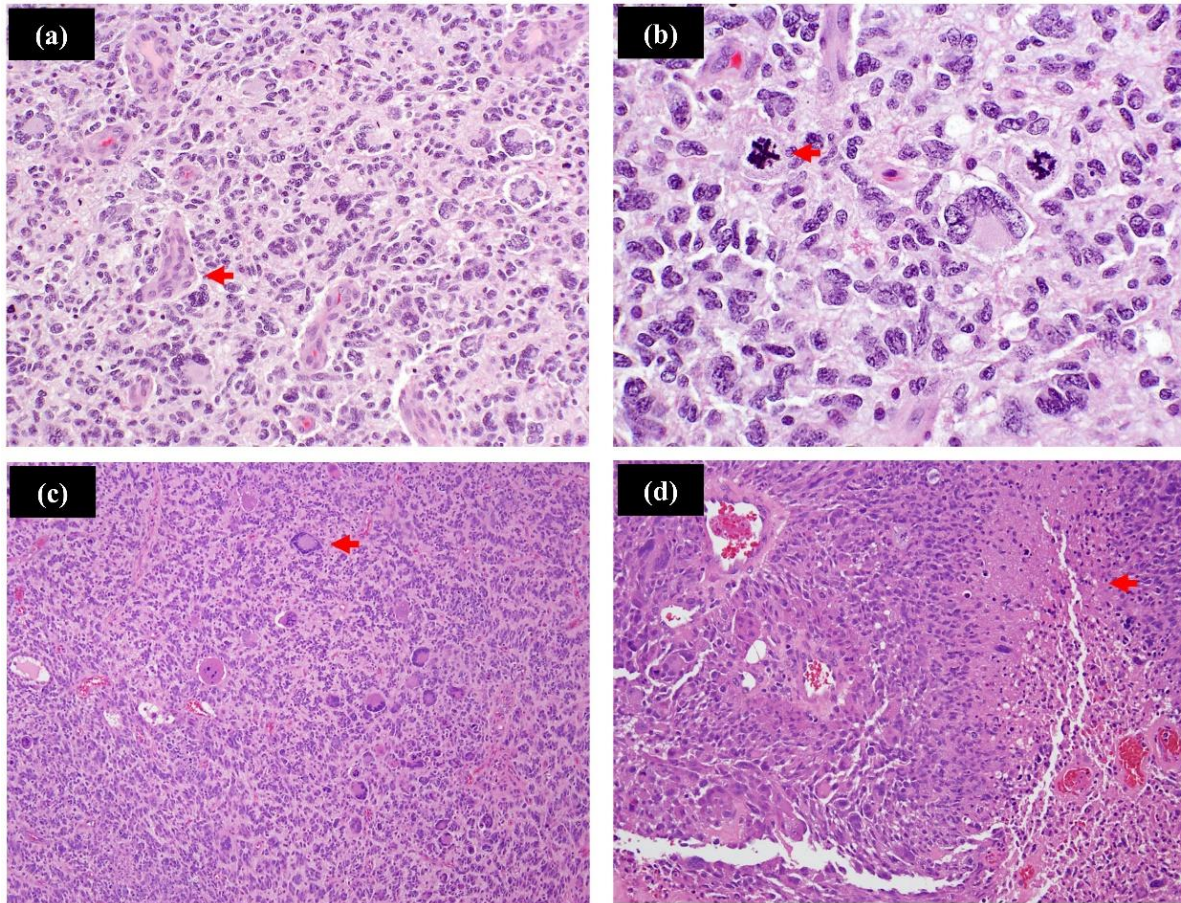


Figure 2.1 (a) Haematoxylin and eosin-stained GBM tumour sections reveal a cellular, pleomorphic, glial neoplasm with glomeruloid microvascular proliferation (arrow; 200 \times magnification). (b) Atypical mitotic figures are prominent (arrow; 400 \times magnification). Haematoxylin and eosin-stained sections of another case demonstrate (c) notable nuclear pleomorphism and giant cell features (arrow; 100 \times magnification), along with (d) pseudopalisading necrosis (arrow; 200 \times magnification). Images are from Whitfield and Huse, 2022.

2.2.2 Molecular biomarkers

The 2016 CNS WHO edition was the first to incorporate molecular parameters into the century-old, microscopy-based diagnostic criteria, classifying GBM as either wt-*IDH* or mutant (mut)-*IDH* (Louis *et al.*, 2016). However, wt-*IDH* GBM develops rapidly *de novo*, without a precursor lesion, whereas mut-*IDH* GBM typically evolves from low-grade diffuse or anaplastic astrocytoma (Ohgaki and Kleihues, 2013). In WHO CNS5, GBM is classified only as “wt-*IDH*”, and mut-*IDH* astrocytoma covers grades 2–4, with no CNS WHO grade 1. The terms mut-*IDH* “GBM” and “anaplastic astrocytoma” have been dropped.

WHO CNS5 specifies several key diagnostic genes (Figure 2.2). In the absence of *IDH* mutations, either telomerase reverse transcriptase (*TERT*) promoter mutations, the combination of chromosome (Chr) 7 gain and Chr 10 loss, or epidermal growth factor receptor (*EGFR*) amplification is considered sufficient molecular evidence of GBM with similar clinical outcome, even when histologic examination meets only WHO grade 2 or 3 criteria (i.e., absence of high-grade features such as microvascular proliferation and/or necrosis (Brat *et al.*, 2018; Tesileanu *et al.*, 2020; Wen *et al.*, 2020). Other biomarkers include p53 (with rare positive cells) and alpha-thalassemia/mental retardation syndrome X-linked (retained nuclear expression) (Osborn *et al.*, 2022).

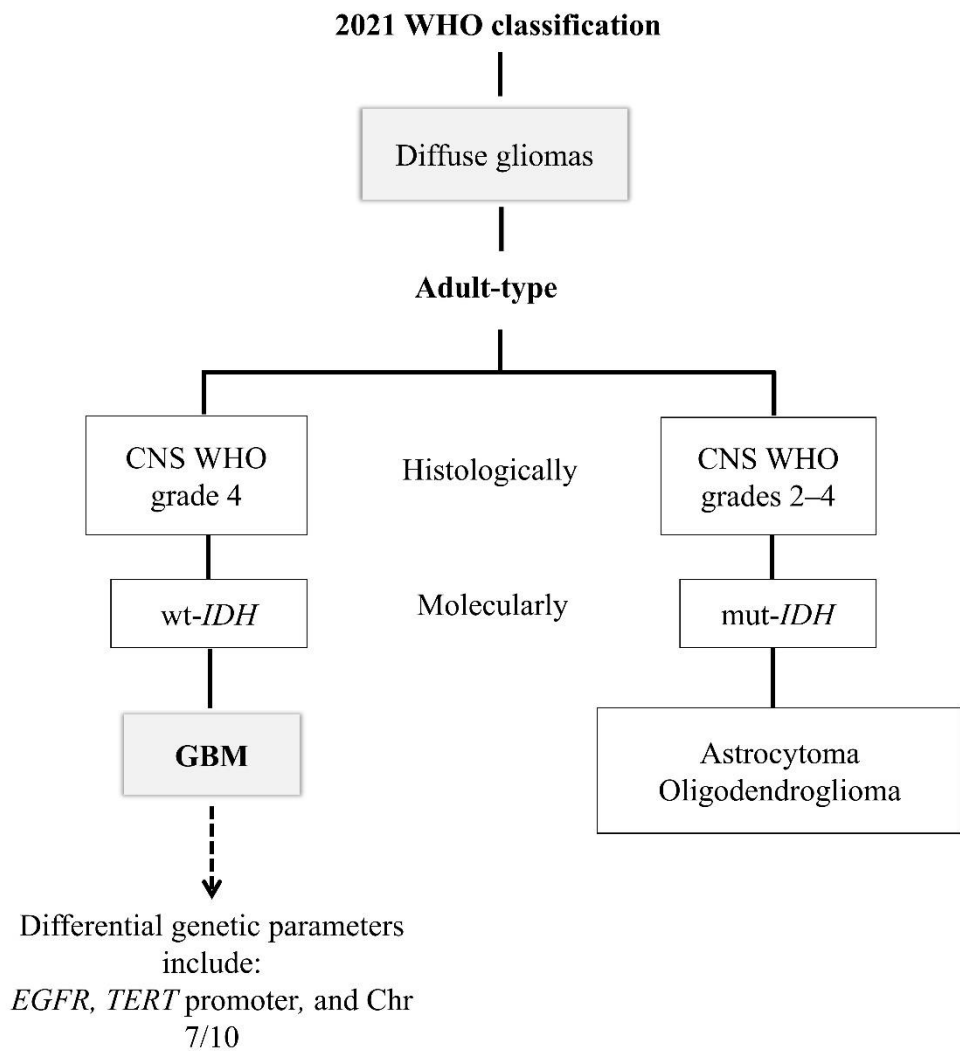


Figure 2.2 Overview of selected diffuse gliomas and key diagnostic genes.
Adapted from Louis *et al.*, 2021.

Presently, molecular patterns serve not only diagnostic but also prognostic and predictive functions. Prognostic biomarkers address clinical outcomes regardless of therapy, whereas predictive ones describe the likelihood of response to a therapeutic intervention. In an Italian single-centre, retrospective cohort study ($n=417$), the most common “druggable” drivers in both newly diagnosed and relapsed GBM were cyclin-dependent kinase inhibitor 2A (*CDKN2A*) loss (54.4%), *CDKN2B* loss (51.8%), *EGFR* amplification (40.3%), and phosphatase and tensin homologue (*PTEN*) loss (43.6%) and mutation (34.3%) (Padovan *et al.*, 2023). Another Italian retrospective cohort

study ($n=120$) found that relapsed GBM patients with methylated O6-methylguanine-DNA methyltransferase (*MGMT*) survived longer than those with unmethylated status (Bosio *et al.*, 2023).

In a retrospective cohort study of Japanese patients with newly diagnosed GBM ($n=100$), unmethylated *MGMT* (49.0%) and *CDKN2A* homozygous deletion (39.0%) were substantially associated with poor prognosis. On the other hand, *TERT* mutation (63.0%), *PTEN* loss (58.0%), *TP53* loss (36.0%), and *EGFR* amplification (19.0%) were not significant predictors of poor prognosis (Funakoshi *et al.*, 2021). In a Chinese retrospective cohort study, *MGMT* methylation predicted longer overall survival (OS) ($n=191$), whilst a higher ki-67 index and *TP53* alterations were among the factors linked to shorter OS ($n=45$) (Guo *et al.*, 2023). In the Indonesian cohort, ki-67 expression was markedly higher in wt-*IDH* than in mut-*IDH* gliomas (Malueka *et al.*, 2020).

To the best of our knowledge, prognostic and predictive factors in a cohort of Malaysian patients with GBM are poorly reported. In a single-centre, cross-sectional study, EGFR (77.8%) and p53 proteins were highly expressed in Malaysian patients with GBM (Azman *et al.*, 2022). Notably, the current progress in biomarker discovery for the prognosis and treatment of GBM is unsatisfactory, largely due to selection bias in clinical and translational research. To address this matter, liquid biopsy studies, such as cerebrospinal fluid and blood sampling, could serve as alternatives to post-operative tumour tissue-based molecular approaches (Pasqualetti *et al.*, 2023).

2.2.3 Treatments and management

The standard of care for newly diagnosed GBM involves surgery, followed by RT with concomitant and adjuvant TMZ. The median OS is 14.6 months (18.8, 13.5, and 9.4 months for patients with complete resection, partial resection, and biopsy alone, respectively) and the median progression-free survival (PFS) is 6.9 months (Stupp *et al.*, 2009; Stupp *et al.*, 2005). However, total resection is frequently impeded by the highly infiltrative nature of GBM cells, and nearly all patients experience relapse after standard treatment (Lim *et al.*, 2022). When it recurs, the survival period is often much shorter, and since none of the current therapies are curative, the National Comprehensive Cancer Network recommends clinical trials as the preferred option for eligible patients (Nabors *et al.*, 2020). Notably, a systematic review and meta-analysis delineated that extending adjuvant TMZ beyond the customary 6-cycle regimen to 7-12 cycles did not improve median OS or PFS in newly diagnosed GBM (Attarian *et al.*, 2021).

Despite decades of diligence, survival rates for newly diagnosed or relapsed GBM have barely awe-inspiring, with many single-agent trials yielding disappointing results (Gatto *et al.*, 2023). Combinatorial approaches have thus far provided only a marginal survival advantage over the standard Stupp protocol. In a multicentre phase 3 randomised clinical trial involving newly diagnosed WHO grade 4 gliomas, TMZ+ interferon alfa (an immunotherapeutic cytokine) resulted in a slightly longer median OS than TMZ alone (20.5 vs. 17.7 months). However, the median PFS was 12.0 and 12.8 months, respectively (Guo *et al.*, 2023a). In newly diagnosed GBM with a methylated MGMT promoter, the median OS was 28.9 months with nivolumab (a programmed death-1 inhibitor)+RT+TMZ, compared to 32.1 months with placebo+RT+TMZ (Lim *et al.*, 2022). In addition, a phase 1 trial of chimeric antigen receptor

T-cell-EGFR variant III+pembrolizumab demonstrated safety and biological activity but lacked efficacy, with median OS and PFS of 11.8 and 5.2 months, respectively (Bagley *et al.*, 2024).

In recurrent GBM, no single treatment regimen provides a marked OS benefit, with median OS ranging from 3 to 17.6 months across chemotherapy, immunotherapy, antiangiogenic, and targeted therapies (Fazzari *et al.*, 2022). For example, in a phase 3 randomised clinical trial, patients with relapsed GBM who received either nivolumab or bevacizumab (an antiangiogenic agent) exhibited equivalent median OS (9.8 vs. 10.0 months) (Reardon *et al.*, 2020). For patients with recurrent or refractory GBM, metformin+TMZ did not provide a clinical benefit when compared to the control arm (placebo+TMZ). Median OS was 17.22 vs. 7.69 months ($P = 0.473$), and median PFS was 2.30 vs. 2.66 months ($P = 0.679$) (Yoon *et al.*, 2023). Besides, a phase 1 clinical trial of dose-escalated oral renin-angiotensin system modulators indicated a 5.3-month increase in survival (median OS was 19.9 months) for patients who relapsed after standard treatment (O'Rawe *et al.*, 2022).

Overall, treatment recommendations for both newly diagnosed and recurrent GBM consider factors such as age, performance status, and genotype (e.g., MGMT promoter methylation status) (Mazarakis *et al.*, 2024; Tan *et al.*, 2020). Older age, male sex, and tumour involvement in deep brain structures or functional areas are associated with a poor prognosis. Conversely, MGMT promoter methylation, maximal tumour resection, and treatment based on the Stupp protocol are predictors of better survival. Additionally, the most common clinical manifestations at diagnosis include intracranial hypertension, a history of epilepsy, motor dysfunction, and aphasia (acquired language disorders) (Guo *et al.*, 2023b). It is worth noting that an important aspect limiting the development of more effective therapies for GBM is the slow and

inefficient clinical trial process (Wen *et al.*, 2020). Many factors contribute to poor trial accrual, including limited awareness and understanding of clinical trial opportunities among patients, together with a lack of knowledge and information about available trials among clinicians (Lee *et al.*, 2019).

2.3 Therapeutic challenges in glioblastoma

2.3.1 Cell cycle dysregulation and apoptosis evasion

Mutations or other alterations in proto-oncogenes and tumour suppressor genes are frequently the starting point (molecular basis) for cancer, with tumour development and apoptosis evasion intimately entwined, conferring cell immortality (Emmanuel *et al.*, 2020). Essentially, cancer is driven by oncogenes (activated and phenotypically dominant) and tumour suppressor genes (inactivated and phenotypically recessive) (Nenclares and Harrington, 2020). In normal cellular processes, proto-oncogenes are key regulatory factors, acting as growth factors, transducers of cellular signals, and nuclear transcription factors. For example, in mitogen signal transduction, key proto-oncogenes include cyclin-dependent kinase 4 (*CDK4*), myelocytomatosis (*MYC*) (a transcription factor), B-cell lymphoma 2 (*BCL2*) (which inhibits apoptosis), and mouse double minute 2 homologue (*MDM2*) (which regulates transcription and binds to the p53 protein, encoded by *TP53*). The activation of these genes into oncogenes can occur via point mutations, chromosomal translocations, and gene amplifications (Emmanuel *et al.*, 2020). Tumour suppressor genes, in contrast, function to inhibit cell proliferation and survival. They are involved in regulating cell cycle progression and apoptosis, thereby providing protection against neoplasia (Nenclares and Harrington, 2020).

For example, the top mutated tumour suppressor genes identified in GSCs derived from patients include *TP53*, followed by *PTEN*, and retinoblastoma 1 (*RBI*) (Lazzarini *et al.*, 2023). In particular, *TP53* mutations contribute to two major clusters of gene expression changes, specifically those related to the cell cycle and proliferative activity. Downstream components of the *TP53* signalling pathway include *CDKN1A* (which encodes p21) and *CDKN2A* (which encodes p16/p14), whilst upstream components encompass checkpoint kinases 1 and 2 (*CHEK1/2*). Notably, *TP53* mutations, whether gain of function (GOF) or non-GOF, exhibit no discernible differences in the gene expression profile of the *TP53* pathway; both types result in functional loss of downstream genes (Sasaki *et al.*, 2023). Moreover, GOF activities of mut-*TP53* are not universally required to sustain tumour growth; removal of mut-*TP53* does not affect the proliferation, survival, or mitochondrial activity of malignant cells (Wang *et al.*, 2024).

At its core, malignant proliferation is driven by cell cycle dysregulation, with most cancers exhibiting alterations in cyclins, cyclin-dependent kinases (CDKs), and CDK inhibitors. In GBM, one study reported enriched biological processes, including upregulated terms related to the cell cycle, specifically the G1/S and G1/M transitions of the mitotic cell cycle (Petkovic *et al.*, 2023). In essence, the cell cycle is a background force underlying the development of multicellular organisms, tissue homeostasis, and tissue repair following injury. When a cell enters the cell cycle, it replicates its genome and segregates the resulting two copies into the daughter cells during mitosis (M). At the core of the molecular network controlling the cell cycle, CDKs function as oscillators, ensuring orderly and tightly regulated progression through the G1, S, G2, and M phases (see Figure 2.3) (Koliopoulos and Alfieri, 2022).

Primarily, cell cycle regulation and deoxyribonucleic acid (DNA) replication are the processes most prominently associated with p53-p21 targets (Engeland, 2022).

As a case in point, loss of p53 or RB function leads to cell cycle dysregulation and malignant proliferation; transcriptional regulation of CDK and cyclin genes is subjected to multiple families of regulators, including p53 and RB (Engeland, 2022). The CDK-cyclin complex can phosphorylate RB protein and regulate the cell cycle positively, whereas CDK inhibitors (e.g., p21, p27, p19, and p16) hinder part of the cell cycle process and play a negative regulatory role. For example, p16 inhibits the activity of CDK4, prevents the phosphorylation of RB protein and the release of early region 2 factor, a family of transcription factors that promote downstream cell cycle factors). This, in turn, inhibits the cell life cycle in the G1 phase (Zhang *et al.*, 2021). In a study, AT7519, a multi-CDK inhibitor, was demonstrated to inhibit CDK1/2 phosphorylation, arrest the cell cycle at the G1/S and G2/M phases, induce cell death through apoptosis and pyroptosis pathways, and decrease GBM cell viability and proliferation (Zhao *et al.*, 2023a).

In addition, it is noteworthy that most oncogenes lack the capacity to drive cell proliferation by themselves. Instead, they (when overexpressed) have evolved with intrinsic and self-limiting safe mechanisms, which engage evolutionary dead-ends such as apoptosis and senescence programmes (Casacuberta-Serra *et al.*, 2024). For example, cellular MYC (c-MYC), a member of the MYC oncogene family, is a critical downstream component of the nuclear factor-kappa β (NF κ β) signalling pathway in GBM cells. Knockdown (KD) of c-MYC expression led to suppression of malignant progression in GBM cells, likely due to direct inhibition of oncogenic pathways driven by c-MYC. Whereas inhibition of the NF κ β signalling pathway with JSH-23, a small-molecular inhibitor that specifically blocks NF κ β transcriptional activity, significantly

reduced Ki-67 expression—a marker of proliferation—in U251 GBM xenograft mice overexpressing the long non-coding RNA XTP6, which is a pivotal regulator in sustaining the NFκβ pathway (Xiao *et al.*, 2024). However, both NFκβ and c-MYC are considered “undruggable”. No drugs directly targeting them have been approved for clinical use (Casacuberta-Serra *et al.*, 2024; Guo *et al.*, 2024).

NFκβ, a nuclear transcription factor, also modulates cell death mechanisms, particularly by suppressing apoptosis. For example, NFκβ target genes include anti-apoptotic molecules such as BCL2, B-cell lymphoma-extra-large (BCLXL), and inhibitors of apoptosis. Furthermore, the mitogen EGFR is closely linked with NFκβ, contributing to drug resistance. EGFR activation triggers the extracellular signal-regulated kinase (ERK)/protein kinase B (AKT) axis, which mediates the nuclear translocation of NFκβ. Subsequently, NFκβ enhances the expression of P-glycoprotein (P-gp) (Ma *et al.*, 2024). Collectively, the interplay of various oncogenes and their complementary actions is referred to as oncogenic cooperation, a central concept in the complex landscape of cancer development and progression (Casacuberta-Serra *et al.*, 2024).

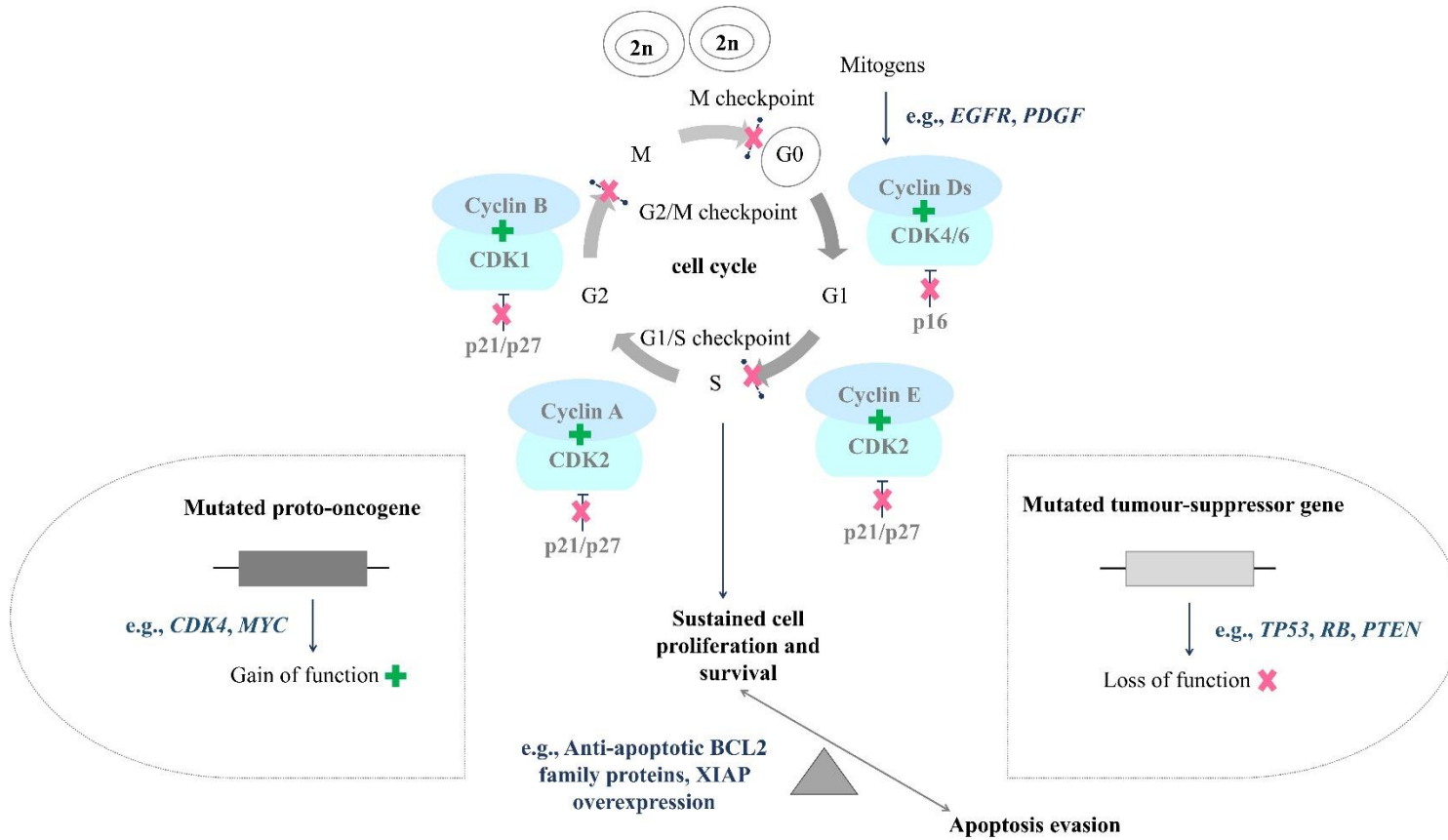


Figure 2.3 Schematic representation of the cell cycle phases along with the respective cyclin-CDK complexes which are necessary for cell cycle progression. G1 (growth phase 1), S (DNA synthesis phase), G2 (growth phase 2), and M, whilst G0 or quiescence (a reversible cycling exit/non-proliferative state). When mitogenic signals trigger proliferation, a complex composed of cyclins and CDKs forms. Abbreviations: PDGF (platelet-derived growth factor); XIAP (x-linked inhibitory apoptosis protein). Adapted from Koliopoulos and Alfieri, 2022; Zhang *et al.*, 2021.

2.3.2 Factors affecting cytotoxic effectiveness

TMZ, an analogue of dacarbazine marketed as Temodar, has been the leading cytotoxic chemotherapeutic in GBM for nearly two decades. Its chemical name is 3-methyl-4-oxoimidaz[5,1-d][1,2,3,5] tetrazine-8-carboxamide, with a molecular weight (MW) of 194.15 g/mol and a chemical formula of C₆H₆N₆O₂. It is a small alkylating molecule and oral prodrug that introduces methyl groups to O6-guanine, N7-guanine, and N3-adenine DNA bases (Teraiya *et al.*, 2023). However, its effectiveness is often limited by resistance mechanisms involving various proteins and signalling pathways (Pinevich *et al.*, 2023). In particular, the durability of cytotoxic chemotherapy in GBM encounters multi-pathway hurdles. This section highlights some factors that can undermine the effectiveness of interventions.

2.3.2(a) Blood-brain barrier

One of the biggest handicaps in attaining optimal therapeutic effectiveness is the difficulty of drugs passing through the blood-brain barrier (BBB), a unique and challenging biological barrier. Doxorubicin, for example, exhibits prominent cytotoxic effects in U87 cell two-dimensional (2D) monolayers and 3D spheroids. However, its therapeutic potential is constrained by poor penetration across the BBB (Janjua *et al.*, 2021). Likewise, curcumin exhibits potential for anti-GBM activity, but it cannot cross the BBB and has poor oral absorption (Mohamadian *et al.*, 2022; Shabaninejad *et al.*, 2020). TMZ, on the other hand, features excellent oral bioavailability (almost 100.0% absorption into the bloodstream) and linear plasma pharmacokinetics, but only 20.0-30.0% crosses the BBB in adults, and 37.0% in paediatric CNS tumour patients (Büscher *et al.*, 2022). To overcome this limitation, various breakthroughs have been made, including nanoparticle-based TMZ delivery systems. Preclinical studies have

demonstrated the potential of polymeric, inorganic, lipid-based, and carbon-based nanoparticles for improving drug effectiveness and biocompatibility (Pourmadadi *et al.*, 2023). Importantly, nano-delivery technologies enable prolonged drug release, thereby maximising therapeutic effects (Zhao *et al.*, 2023b).

For example, compared to free TMZ, TMZ-loaded liposomes, TMZ-loaded polyethylene glycol (PEG)ylated liposomes, TMZ-loaded lyotropic liquid crystals (LLC), and TMZ-loaded PEGylated LLC all exhibited increased cytotoxicity in U87 cells after 48 h at 0.2 or 1.0 mM. In terms of pharmacokinetics, TMZ-loaded PEGylated liposomes and PEGylated LLC display lower clearance, higher plasma concentrations up to 6 h (0.84 and 1.54 μ g/ml), and longer half-lives (1.64 and 2.61 h) vs. free TMZ (0.56 μ g/ml and 1.31 h), respectively. Both formulations also showed increased brain bioavailability, with area under curve (AUC)_{0- ∞} values of 18.20 and 25.49 μ g/ml^{0.5}h compared to free TMZ (14.27 μ g/ml^{0.5}h). Additionally, coated TMZs resulted in \approx 3-fold reduced uptake by macrophage cells, thereby extending plasma circulation (Waghule *et al.*, 2023).

Besides, ultra-small, large pore silica (USLP) nanoparticles loaded with TMZ, reinforced with cationic amino (NH₂) group, surface PEGylated (to minimise efflux), and/or cascade targeting protein lactoferrin (LF) (to maximise delivery into GBM). Both TMZ formulations, i.e., USLP-NH₂-PEG-TMZ and USLP-NH₂-PEG-TMZ-LF, markedly increased late and early apoptotic death in U87 and murine glioma 261 cells, respectively, when compared to free TMZ. In an *in vitro* BBB model, these USLP formulations did not enhance the TMZ delivery but greatly reduced efflux. Further, *in vivo* studies evidenced the biocompatibility of USLP-based delivery. Intravenous administration of USLP particles at 50 mg/kg resulted in significant accumulation in the brain within a few hours, with no apparent pathophysiological changes in vital

organs (Janjua *et al.*, 2023). Another great effort is chitosan- β -glycerophosphate-based thermogel (THG) containing TMZ-loaded mesoporous silica (SiO_2) nanoparticles (TMZ-THG- SiO_2) or polycaprolactone (PCL) microparticles (TMZ-THG-PCL). The biocompatibility of THG with brain tissue was demonstrated, and both encapsulation formulations showed significant *in vitro* cytotoxicity and *in vivo* anti-tumour efficacy, with delayed tumour recurrence in an orthotopic xenograft resection and recurrence mouse model using U87-Red-Fluc cells (Gherardini *et al.*, 2023).

Notwithstanding, nanocarriers still have some drawbacks, including poor drug penetration, limited drug encapsulation, and poor targeting (Priya *et al.*, 2022). For example, local chemotherapy of brain tumours is often released from the carrier before it comes into contact with the cancer cells (Liu *et al.*, 2023a). These limitations can be addressed through surface modifications (engineered coatings), which make possible controlled release, greater penetration efficiency, and targeted drug delivery (Priya *et al.*, 2022). Notably, a thorough review article highlights that emulsomes provide advantages over other lipid-based drug delivery systems (Table 2.2) (Singh *et al.*, 2023). Emulsomes, a modified generation of liposomes and considered a nexus between liposomes and solid lipid nanoparticles, can improve pharmacokinetics, enhance therapeutic efficacy, and combat multidrug resistance (Elnady *et al.*, 2023).

Of note, various clinical trials involving TMZ are ongoing, but only a small number of nanoformulations have advanced to phase 1 and 2 studies in patients with HGG. These include liposomal curcumin paired with RT and TMZ (NCT05768919, newly diagnosed cases) and rhenium-186 nanoliposomes (NCT01906385, relapsed cases) (last accessed *clinical trials.gov* on 10th Sept 2023). Other liposome-based studies include mitoxantrone hydrochloride (HCl) (phase 1/2), doxorubicin HCl (phase 1/2), and paclitaxel (phase 4) (Ashrafizadeh *et al.*, 2022). Besides, collaborative